Single particle ignition and combustion of pulverized pine wood, wheat straw, rice husk and grape pomace

Weng, Wubin; Costa, Mário; Aldén, Marcus; Li, Zhongshan

Published in:
Proceedings of the Combustion Institute

DOI:
10.1016/j.proci.2018.05.095

2019

Single particle ignition and combustion of pulverized pine wood, wheat straw, rice husk and grape pomace

Wubin Weng[1], Mário Costa[2], Marcus Aldeń[1], Zhongshan Li[1]

[1]Division of Combustion Physics, Lund University, Post Office Box 118, SE-221 00 Lund, Sweden
[2]IDMEC, Mechanical Engineering Department, Instituto Superior Técnico, Universidade de Lisboa, Lisboa, Portugal

Corresponding author: Mário Costa; mcosta@ist.utl.pt

Colloquium of research topic: Solid Fuel Combustion

We will pay color reproduction charges

Method 1

Length excluding title block, abstract and separate list of figure captions: 3903 + 2321 = 6224/6200

Main Text: 3903

References: (15 references + 2) x (2.3 lines/reference) x (7.6 words/line) = 297

Table 1: (27 lines + 2 lines) x (7.6 words/line) x (1 column) + 7 words in caption = 227

Figure 1 with caption: (41 mm + 10 mm) x (2.2 words/mm) x (1 column) + 22 words in caption = 134

Figure 2 with caption: (53 mm + 10 mm) x (2.2 words/mm) x (2 column) + 83 words in caption = 360

Figure 3 with caption: (45 mm + 10 mm) x (2.2 words/mm) x (1 column) + 18 words in caption = 139

Figure 4 with caption: (96 mm + 10 mm) x (2.2 words/mm) x (2 column) + 86 words in caption = 552

Figure 5 with caption: (67 mm + 10 mm) x (2.2 words/mm) x (2 column) + 82 words in caption = 421

Figure 6 with caption: (65 mm + 10 mm) x (2.2 words/mm) x (2 column) + 61 words in caption = 191

Submitted to Proceedings of the Combustion Institute

May, 2018

ABSTRACT

This work examines the combustion behavior of single pulverized biomass particles from their ignition to their early stages of char oxidation. The biomass residues investigated were pine wood, wheat straw, rice husk and grape pomace. The biomass particles, in the size range 224-250 μm, were injected upward into a confined region with hot combustion products, produced by a flat flame McKenna burner, with a mean temperature of 1610 K and a mean O_2 concentration of 6.5 vol.%. Temporally and spectrally resolved images of the single burning particles were recorded with an ICCD camera equipped with different band-pass spectral filters. Data are reported for CH*, C_2*, Na* and K* chemiluminescence, and thermal radiation from soot and char burning particles. The data on CH* and C_2* chemiluminescence and soot thermal radiation permits to identify important differences between the ignition delay time, volatiles combustion time and soot formation propensity of the four biomass residues, which are mainly affected by their moisture and volatile matter contents. The Na* and K* emission signals follow the same trends of the CH* and C_2* emission signals until the end of the volatiles combustion stage, beyond which, unlike the CH* and C_2* emission signals, they persist owing to their release from the char burning particles. Moreover, during the volatiles combustion stage, the Na*/CH* and K*/CH* ratios present constant values for each biomass residue. The CH* and thermal radiation emission data suggest that all biomass char particles experienced heterogeneous oxidation at or immediately after the extinction of the homogeneous volatiles combustion.

Keywords: Biomass residues; single particle combustion; temporally and resolved images; chemiluminescence

1. INTRODUCTION

In a recent study [1], we demonstrated the ability of using temporally and spectrally resolved images, obtained with the aid of an intensified charge-coupled device (ICCD) camera, equipped with various band-pass filters, to gather quantitative information on the combustion behavior of single pulverized biomass (wheat straw) particles, from ignition to char oxidation early stages. In the present work, we extended the analysis to other biomass residues, such as pine wood, rice husk and grape pomace, in order to evaluate if the experimental approach is good enough to capture and quantify the particularities associated with the combustion of different biomass residues, namely in regard to their ignition behavior, devolatilization and volatiles combustion, soot formation propensity, release characteristics of alkaline species, and char oxidation.

In contrast with works on single pulverized coal particles [2-8], previous related studies on the combustion behavior of single pulverized biomass particles are very scarce. Riaza et al. [9] employed three-color pyrometry and high-speed high-resolution cinematography to investigate the combustion behavior of single particles of sugarcane bagasse, pine sawdust, torrefied pine sawdust and olive residue, all in the size range 75-150 μm, in a drop tube furnace, set at 1400 K, in both air and O_2/CO_2 atmospheres. The authors concluded that, in contrast with the combustion behavior of coals, which differs widely with rank, type and seam, the combustion behavior of the four distinct biomass residues evidenced only small differences based on their origin, type and pre-treatment. In particular, they observed that olive residue chars and bagasse chars burned at lower and higher temperatures, respectively, than the other biomass residues. Mock et al. [10, 11] used high-speed photography to examine the burning behavior of single particles of torrefied wood, coffee waste, sewage sludge and torrefied sewage sludge, in size ranges 150-215 μm, 255-300 μm, 355-425 μm and 425-500 μm, in an entrained flow reactor with cross particle injection in combustion products at 1090 K and 1340 K and O_2 concentrations ranging from 10 vol.% to 40 vol.%. The authors observed different burning characteristics (e.g., ignition delay time, flame volatility, soot formation tendency, char oxidation) of the distinct biomass particles, which they attributed to their different chemical and

physical properties. Simões et al. [12] also employed high-speed photography to study the ignition behavior of single particles of wheat straw, kiwi branches, vine branches, sycamore branches and pine bark, in size ranges 80-90 μm, 212-224 μm and 224-250 μm, in a confined laminar flow of combustion products at temperatures ranging from 1500 K to 1800 K and O_2 concentrations ranging from 3.5 vol.% to 6.5 vol.%. The authors concluded that ignition of the biomass particles generally occurred in the gas-phase, and that their ignition delay time decreased as the gas temperature increased. Very recently, Carvalho et al. [13] used the same experimental setup and measuring techniques of Simões et al. [12] to evaluate the effects of K and Ca on the early stages of the combustion of single particles of grape pomace, in the size range 200-250 μm, pre-treated with demineralization and impregnation processes. The authors concluded that the demineralization pre-treatment increased both the ignition delay time and the volatiles combustion time of the single particles, and that both the K and the Ca impregnation pre-treatments decreased the volatiles combustion time as the concentration of K or Ca increased, without a significant impact on the ignition delay time. In the context of single particle biomass combustion, the work of Wornat et al. [14, 15] on biomass chars must be here mentioned. These authors used a variety of analytical techniques to investigate the physical and chemical transformations of pine and switchgrass chars, in a size range 75-106 μm, during combustion at 1600 K in a laminar flow reactor. Their results revealed several important changes in both the organic and inorganic constituents of the chars.

These few studies [9-15] provided essentially qualitative information on the ignition behavior and volatiles combustion of single pulverized biomass particles. In light of this, there is a need not only to obtain quantitative information on these aspects, but also to extend the research on single biomass particles combustion to encompass critical issues such as the release characteristics of alkali species. In the present study, we examine the combustion behavior of single pulverized biomass particles of pine wood, wheat straw, rice husk and grape pomace from ignition to the early stages of the char oxidation. To this end, temporally and spectrally resolved images of the single burning particles were recorded with an ICCD camera equipped with different band-pass spectral filters. Data were obtained for CH*, C_2*, Na* and K* chemiluminescence, and thermal radiation from soot and

char burning particles. To the best of our knowledge this work constitutes the first attempt to measure quantities such as Na* and K* chemiluminescence from a moving single pulverized biomass particle under conditions (e.g., heating rate and temperature) close to those they encountered in real furnaces.

2. MATERIALS AND METHODS

2.1. Experimental setup and optical diagnostics

Figure 1a shows a schematic of the experimental setup used, which is described in more detail elsewhere [12]. It consists of a biomass feeding unit, a McKenna flat flame burner and an air/methane feeding system. The biomass feeding unit consists of a mass flow controller, a 10 mL syringe and a vibrating motor. The biomass particles, stored in the syringe, are fed into a stream of nitrogen and injected upward through a central hole located in the burner (I.D. 1.55-mm) into the hot combustion products region of the McKenna burner. The Mckenna flat flame burner consists of a stainless-steel cylinder enveloping a water-cooled bronze porous sintered matrix of 60-mm diameter. Two mass flow controllers allow the control of the methane and primary air flow rates to the burner. Right above the burner, a high-grade fused quartz of I.D. 70-mm, height of 500-mm, and thickness of 2-mm was used to confine the flow and to avoid the entrainment of ambient air, while providing optical access.

Figure 1b shows a schematic of the optical diagnostics used for the capture of images of the single burning biomass particles [1]. The temporally resolved images of the single burning particles were obtained with an ICCD camera (Andor, iStar, 1024×1024 pixels) with an exposure time of 500 μs. To obtain spectrally resolved images the camera was equipped with different band-pass filters, with bandwidths of 10 nm. Additionally, a stereoscope lens was placed in front of the ICCD camera to allow for the simultaneous capture of images of each particle with two filters. The synchronization between the ICCD camera and each incoming single particle was achieved with the aid of the emission signal synchronization system shown in Fig. 1b. This synchronization system also allowed for the calculation of the residence time of each particle in the hot combustion products region

produced by the McKenna burner. A 532 nm continuous-wave laser (200 mW) was used to generate a laser beam with a diameter of 1-mm. This laser beam was placed very close to the exit of the central hole located in the Mckenna burner through which the particles were injected upward into the hot combustion products region. The scattering emission signal generated by each single particle crossing the laser beam was collected by a photodiode together with a spherical lens, which triggered the ICCD camera through a pulse generator (DG535).

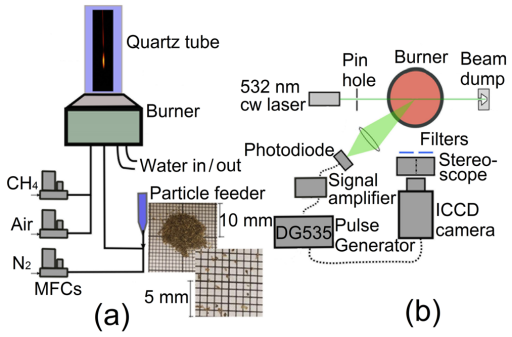

Figure 1. Schematic views of the (a) experimental setup; and (b) optical diagnostics for the capture of images of single burning particles.

2.2 Biomass residues and test conditions

Table 1 shows the properties of the four biomass residues used in this study. All biomass residues were grounded and sieved to a particle size range of 224-250 µm. The particles shape was assessed with a scanning electron microscope through a quantitative analysis of the aspect ratio (ratio between the largest length of the particle and the corresponding perpendicular length) of the particles of each residue for a minimum of 50 particles. The analysis revealed that the pine wood particles had an aspect ratio of ~2 and presented a homogeneous size distribution, while the remaining residues were more elongated (aspects ratios of ~3.5 for wheat straw, ~4 for rice husk and ~3 for grape pomace), with a higher heterogeneity in the size distribution.

The McKenna burner was fed with a mixture of CH_4 (1.03 SL/min) and air (14.68 SL/min). The resulting flat flame, with an equivalence ratio of 0.67, produced a region of hot combustion products, where the particles were injected, with a mean velocity between 0.4 m/s to 0.55 m/s, a

mean temperature of 1610 K and a mean O_2 concentration of 6.5 vol.%. The nitrogen flow rate used to transport the biomass particles was 0.097 SL/min.

Table 1. Properties of the biomass residues.

Parameter	Pine wood	Wheat straw	Rice husk	Grape pomace
Proximate analysis (wt.%, as received)				
Volatile matter	78.1	64.9	64.5	64.7
Fixed carbon	15.2	12.4	12.7	25.0
Moisture	6.3	8.0	10.0	6.6
Ash	0.4	14.7	12.8	3.7
Ultimate analysis (wt.%, dry ash free)				
Carbon	53.8	41.1	42.2	51.3
Hydrogen	7.3	5.3	5.6	6.7
Nitrogen	< 0.05	0.7	0.8	1.9
Sulfur	< 0.02	< 0.02	< 0.02	< 0.02
Oxygen	38.9	52.6	51.1	40.1
Heating value (MJ/kg)				
Low	19.1	13.0	14.6	20.1
High	20.4	14.1	15.8	21.2
Ash analysis (wt.%, dry basis)				
SiO_2	5.8	42.0	86.6	5.5
Al_2O_3	3.7	8.7	1.2	1.0
Fe_2O_3	6.1	5.0	0.5	1.2
CaO	49.5	28.0	1.5	37.8
SO_3	2.6	1.0	0.4	1.7
MgO	19.3	3.7	1.0	7.2
P_2O_5	7.8	2.6	2.2	19.7
K_2O	2.9	6.9	3.6	24.7
Na_2O	1.2	0.6	0.3	0.4
Cl	0.0	0.6	0.5	0.0
Other oxides	1.1	0.9	2.2	0.8

3. RESULTS AND DISCUSSION

The imaging region of the ICCD camera was set to 60 mm × 60 mm, with a spatial resolution of ~58 μm per pixel, and located above the burner in two possible ways: (i) from 0 (burner surface) to 60 mm above the burner surface, or from 30 mm to 90 mm above the burner surface. When a

particle was injected upward into the confined hot combustion products region, the ICCD camera was triggered and generated a burst of exposures of 14 pulses. The time gap between each pulse was 10 ms and the camera exposure time for each pulse was 500 μs. As mentioned earlier, a stereoscope lens was placed in front of the camera to allow for the simultaneous capture of images of each particle with two filters. The 430 nm band-pass filter (BF430, for CH* chemiluminescence) was chosen to pair with the other five filters: 515 nm band-pass filter (BF515, for C_2* chemiluminescence), 589 nm band-pass filter (BF589, for Na* chemiluminescence), 652 nm band-pass filter (BF652, for soot radiation), 766 nm band-pass filter (BF766, for K* chemiluminescence), and a long-pass filter (RG 1000, for char radiation). Therefore, the results obtained with the filter BF430 are used as the reference data for each biomass fuel – the data obtained with this filter in the different filter combinations used was quite similar for a given biomass.

Figure 2 shows sequences of instantaneous images (left) and respective instantaneous emission signal areas (right) of the four burning pulverized biomass particles obtained with the ICCD camera equipped with the 430 nm band-pass filter as a function of the particle residence time in the hot combustion products region. The signal area was determined based on a multi-pixel analysis with a signal to noise ratio over 1.6. The sequences of images illustrate well the volatiles combustion process for the four biomass residues, with the strong CH* chemiluminescence signal being an unambiguous indicator of the occurrence of volatiles combustion. Moreover, the CH* images, more specifically, the temporal evolution of the emission signal area, allow to identify the ignition instant, and hence to calculate the ignition delay time. Here, we established a criterion of 15% of the CH* emission signal area peak to define the ignition delay time for the present biomass residues (see below).

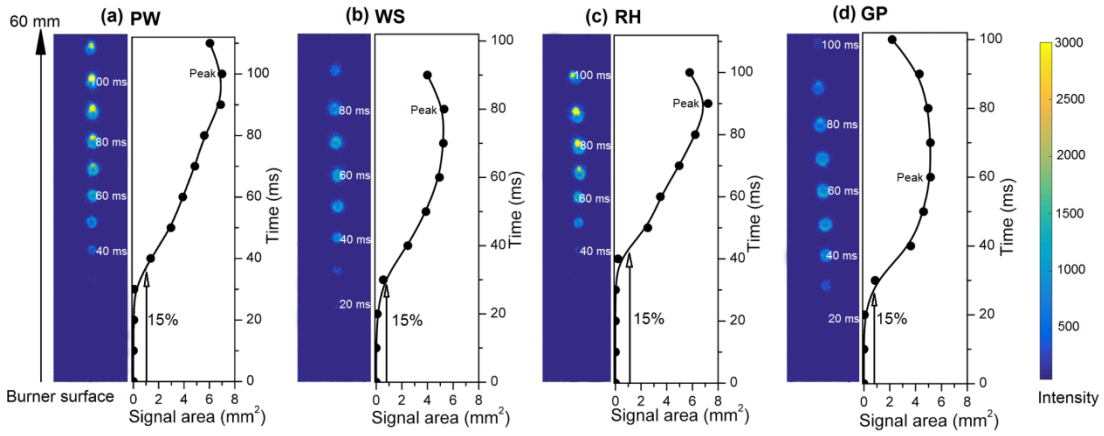

Figure 2. Sequences of instantaneous images (left) and respective instantaneous emission signal areas (right) of the four burning pulverized biomass particles obtained with the ICCD camera equipped with the 430 nm band-pass filter as a function of the particle residence time in the hot combustion products region. (a) Pine wood (PW); (b) wheat straw (WS); (c) rice husk (RH); (d) grape pomace (GP). In the emission signal area curves, the location of the peak value and 15% of the peak value are indicated.

Figure 3 shows the particle velocity of the four burning pulverized biomass particles as a function of the residence time. The particles velocity was calculated based on the time interval of 10 ms and the flying distance in this time interval of, at least, 100 particles for each residue. The mean velocity of the burning biomass particles during the volatiles combustion stage was ~0.6 m/s, as shown in the dashed marked region of Fig. 3, which was close to the flue gas velocity. In general, the particle velocity of the four biomass residues decreases initially in the preheating region from ~0.7-0.8 m/s (the transport fluid flow has an initial velocity of ~0.8 m/s) down to ~0.5-0.6 m/s, remains approximately constant up to 70 ms, beyond which it increases significantly up to the early stages of the char oxidation stage.

Figure 3 also reveals that the particle velocities are slightly different for the four biomass residues. Initially, the rice husk particles present higher velocities than all the others, but after ignition the grape pomace particles travel faster than the remaining ones. The reasoning for this

different behavior is presumably related with particle shape and density, and ignition delay time, but with the information available, we are unable to provide a definitive explanation.

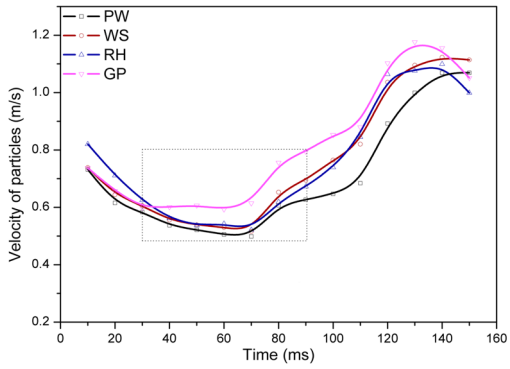

Figure 3. Particle velocity of the four burning pulverized biomass particles as a function of the residence time.

Figure 4 shows average emission signal area (left) and emission signal value (right) of the four burning pulverized biomass particles obtained with the ICCD camera equipped with different pairs of filters as a function of the particle residence time in the hot combustion products region. The signal value was taken as the sum of the signal intensity of the pixels in the signal area. The data points included in Fig. 4 were obtained from the average of measurements from 100 particles. Overall, the figure reveals that the main difference between the 430 nm (CH*), 515 nm (C2*) and 652 nm (soot) signals relates with the time of their initial appearance, with the soot thermal radiation signal being slight delayed in relation to the other two signals. This is because the amount of volatile matter released from the particles at the beginning of the combustion process being small and the amount of O_2 in the hot combustion products being enough to inhibit soot formation.

Figures 4a and 4d reveal that the CH* emission signal peaks obtained with the 430 nm band-pass filter from the particles of pine wood and rice husk are higher than those obtained from the particles of wheat straw and grape pomace. This is due to the soot thermal radiation interference, as can be clearly observed in Figs. 2a and 2c. Moreover, it is observed that this interference is much less accentuated in the emission signal area curves than in the emission signal value curves. Both the

wheat straw and grape pomace particles present CH* emission signal area peaks at ~4 mm^2, with negligible soot thermal radiation interference.

Using the criterion for ignition delay time introduced earlier (15% of the CH* emission signal area peak), the calculated average ignition delay times for the particles of pine wood, wheat straw, rice husk and grape pomace were 27 ms, 27 ms, 33 ms and 18 ms, respectively. These values were calculated based on, at least, 100 particles, which was high enough to guarantee statistical significance of the ignition delay time results. Similar ignition delay times can be calculated from the CH* emission signal value curves (Fig. 4d) since there was no soot formation in these early stages of the combustion process. The ignition delay times calculated here are in line with those reported by Simões et al. [12] for some of these biomass residues in the same experimental setup but using an ignition criterion based on the visible light emission signal (15% of the maximum luminosity intensity).

Table 1 shows that wheat straw, rice husk and grape pomace present similar volatile matter contents, but slightly different moisture contents, which influence the ignition delay time – the higher the moisture content (rice husk), the higher the ignition delay time. In order to quantify the impact of the moisture on the ignition delay times, the drying times were estimated based on the diffusion of water vapor from the surface of the particle to the surroundings following the methodology used by Simões et al. [12]. The calculated drying times for the particles of pine wood, wheat straw, rice husk and grape pomace were 3.3 ms, 4.2 ms, 5.2 ms and 3.4 ms, respectively. This indicates that the relatively small differences in the moisture content of the four residues do not affect the qualitative relation among the calculated ignition delay times from the present data.

In comparison with the pine wood, the wheat straw, rice husk and grape pomace have less volatile matter in their composition, which is reflected in the duration of their volatiles combustion stages. For these three biomass residues the volatiles combustion stage ends at ~110 ms, while for pine wood it ends above 140 ms, as seen in Fig. 2a.

For the C_2* emission signal obtained with the ICCD camera equipped with the 515 nm band-pass filter, the interference from soot thermal radiation is stronger in the case of the pine wood and

rice husk particles. For the particles of wheat straw and grape pomace, the C_2* emission signals disclose similar volatile flame sizes as those revealed by the CH* emission signals. Fig. 4 also shows that the 652 nm band-pass filter captured the soot thermal radiation from the four burning pulverized biomass particles. It is observed that significantly more soot is formed during the burning of the pine wood and rice husk particles than during the burning of the wheat straw and grape pomace particles, presumably due the nature of the volatiles, including that of the tars, released from the biomass particles. For all biomass residues, the soot formation and oxidation initiates usually ~10 ms after ignition. Note that the emission signals observed in Figs. 4c and 4f after the end of the devolatilization stage result from the thermal radiation of the burning char particles. It is observed that the signal areas are larger than the size of the char particles, because of the error introduced by the extremely high signal from the burning char particles when the 652 nm band-pass filter was used. This strong signal was surrounded by strong noise due to its overflowing on the ICCD camera. As the strong noise was counted as signal, the signal area value became larger than the true value. However, the correct size of the burning char particles can be easily obtained as filter RG 1000 was used (see below).

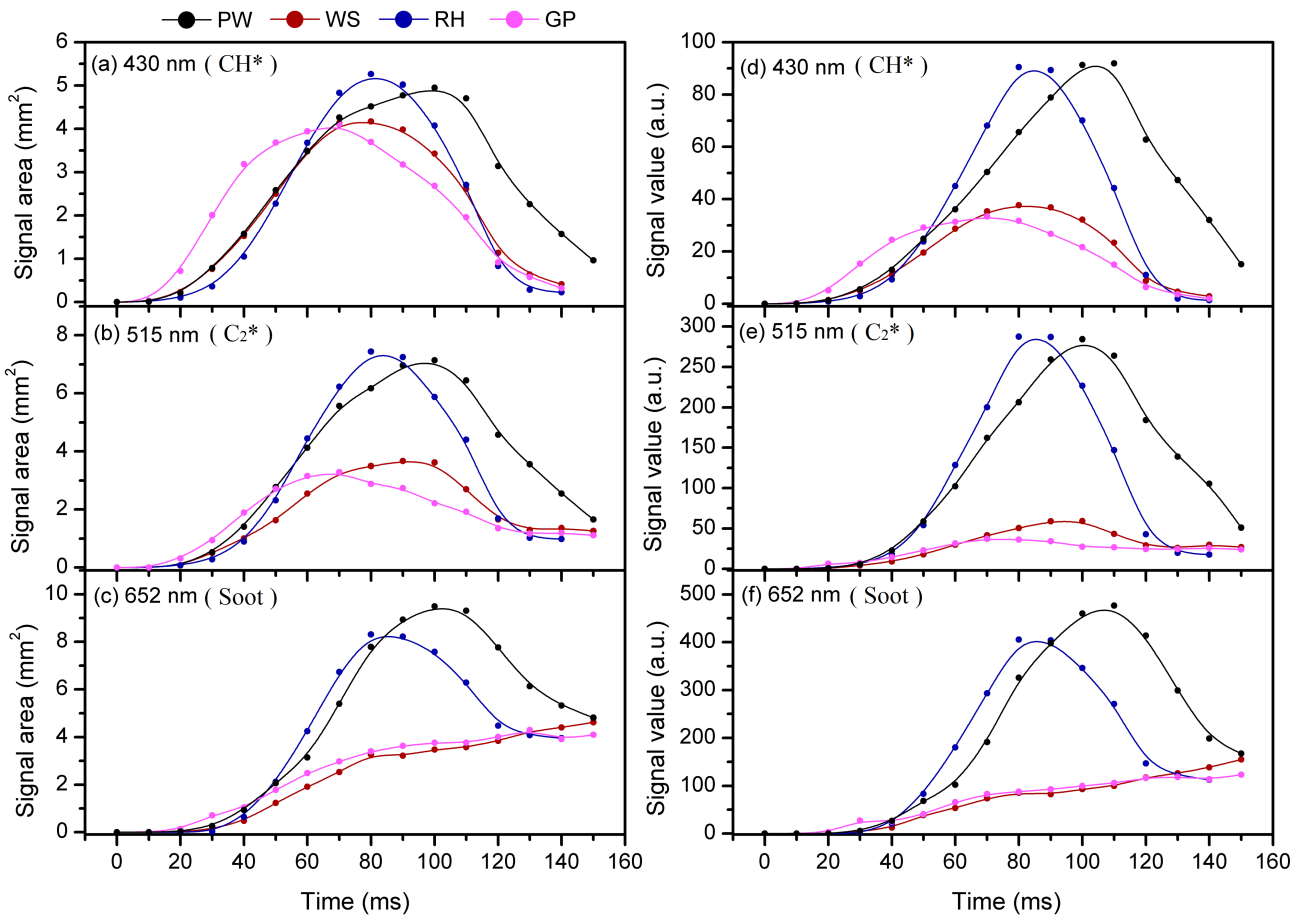

Figure 4. Average emission signal area (left) and emission signal value (right) of the four burning pulverized biomass particles obtained with the ICCD camera equipped with different pairs of filters as a function of the particle residence time in the hot combustion products region. (a) Emission signal area with 430 nm (CH*); (b) emission signal area with 515 nm (C_2*); (c) emission signal area with 652 nm (soot); (d) emission signal value with 430 nm (CH*); (e) emission signal value with 515 nm (C_2*); (f) emission signal value with 652 nm (soot).

The sodium and potassium release rates of the four burning pulverized biomass particles were evaluated through the Na* and K* emission signal areas. Figure 5 shows average emission signal area (left) and emission signal area ratio (right) of the four burning pulverized biomass particles obtained with the ICCD camera equipped with the pair of filters 589 nm/430 nm and 766 nm/430 nm as a function of the particle residence time in the hot combustion products region. The strength of the emission signals showed in Fig. 5 is related with the sodium and potassium release rates from the burning particles, but they are also influenced by the volatiles combustion intensity. Indeed, the

evolution of the Na* and K* emission signals in Fig. 5 is similar to that of the CH* and C_2* emission signals in Fig. 4 during the volatiles combustion stage. After the end of this stage, however, the Na* and K* emission signals persist, revealing their release from the char burning particles, while the CH* and C_2* emission signals disappear, as expected. We can anticipate with reasonable justification that larger Na* and K* emission signal areas indicate larger amounts of sodium and potassium released from the particles since the four biomass residues have similar volatiles combustion intensity, as typified by the similar CH* emission signal peaks observed in Fig. 2. In order to eliminate the effect of the volatiles combustion intensity, the measured Na* and K* emission signals were divided by the measured CH* emission signal, as represented in Figs. 5c and 5d. It is seen that during all the volatiles combustion stage, after the ignition, i.e., from residences times of 30 ms to ~110 ms, each biomass residue present constant ratios, which indicates a stable release of sodium and potassium. At residence times of ~110 ms, the abruptly increase of the ratios for the particles of wheat straw, rice husk and grape pomace indicates the initiation of the char oxidation stage. Note that in the case of the pine wood particles, the char oxidation initiates at a residence time of ~140 ms (cf. Fig. 5), due to the larger volatile matter content present in this biomass residue (cf. Table 1). Further evidence of the initiation of the char oxidation is provided in the following paragraph.

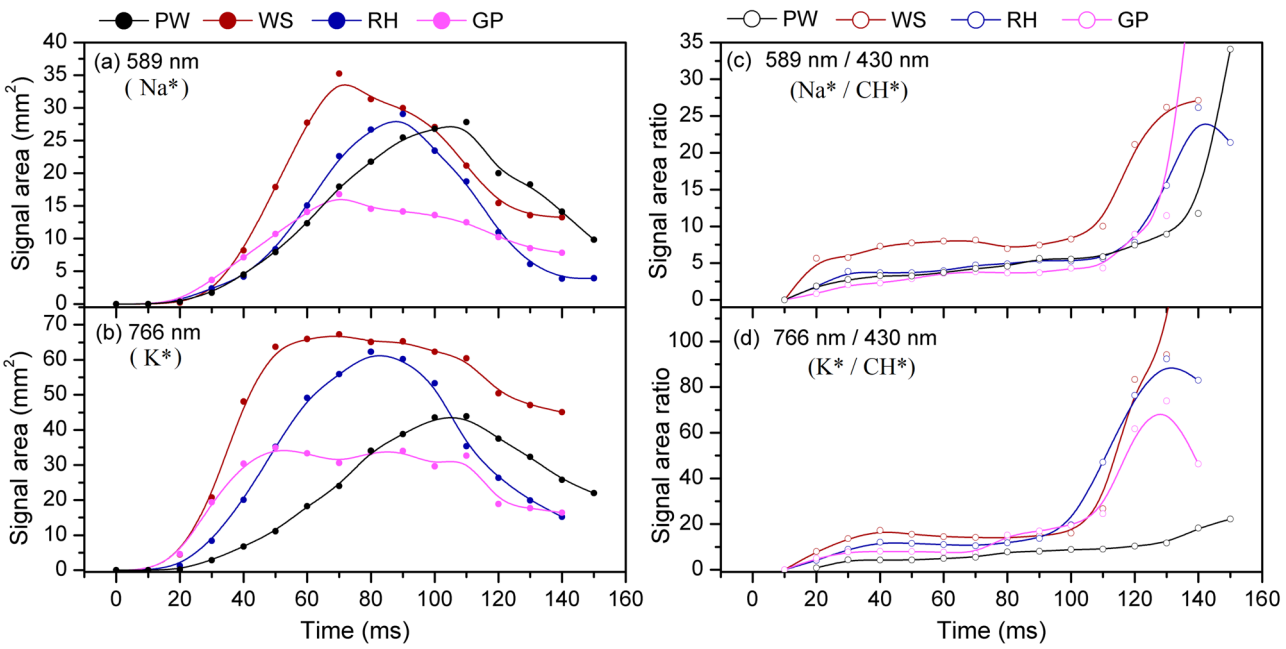

Figure 5. Average emission signal area (left) and emission signal area ratio (right) of the four burning pulverized biomass particles obtained with the ICCD camera equipped with the pair of filters 589 nm/430 nm and 766 nm/430 nm as a function of the particle residence time in the hot combustion products region. (a) Emission signal area with 589 nm (Na*); (b) emission signal area with 766 nm (K*); (c) emission signal area ratio 589 nm/430 nm (Na*/CH*); (d) emission signal area ratio 766 nm/430 nm (K*/CH*).

The present setup allows for the examination of the early stages of the oxidation of the char particles. Fig. 6 shows typical sequences of instantaneous images (left) and respective normalized instantaneous emission signal value (right) of three burning pulverized biomass particles obtained with the ICCD camera equipped with the pair of filters RG 1000/430 nm as a function of the particle residence time in the hot combustion products region. Note that in these cases (particles of wheat straw, rice husk and grape pomace) the emission signals were captured for particles residence times above ~80 ms (30 mm above the burner). For these biomass particles, the volatiles combustion stage, as typified by the CH* emission signal, ended at residence times of ~110 ms, when the thermal radiation emission signal of the burning char particles started to be captured. Both the CH* and thermal radiation emission signals suggest that all biomass char particles experienced heterogeneous

oxidation at or immediately after the extinction of the homogeneous volatiles combustion. In the case of the rice husk particles, it is possible to observe (Fig. 6b) that the thermal radiation emission signal, originated from soot burning, decreases to almost zero at a residence time of ~110 ms, followed by a rapid increase of the thermal radiation due to the onset of the char oxidation stage. In the cases of the wheat straw and grape pomace particles, the emission data in Figs. 6a and 6c suggest a very small overlap between the end of the volatiles combustion stage and the onset of the char oxidation stage.

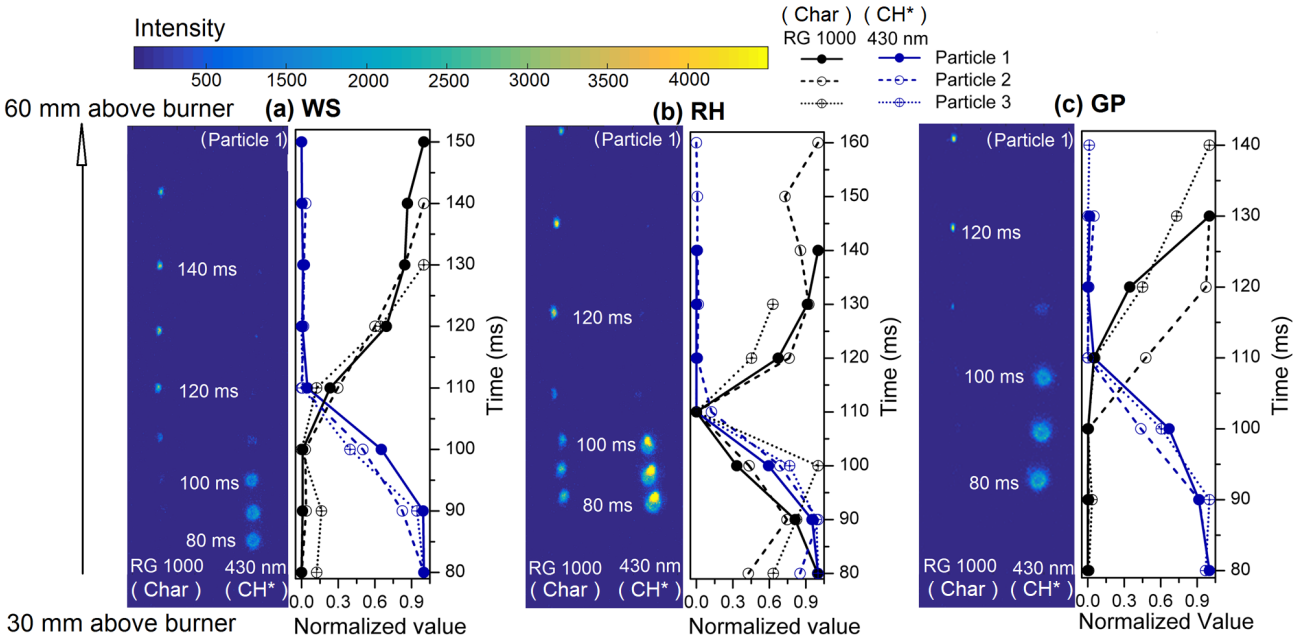

Figure 6. Typical sequences of instantaneous images (left) and respective normalized instantaneous emission signal value (right) of three burning pulverized biomass particles obtained with the ICCD camera equipped with the pair of filters RG 1000/430 nm (char/CH*) as a function of the particle residence time in the hot combustion products region. (a) Wheat straw (WS); (b) rice husk (RH); (c) grape pomace (GP).

4. CONCLUSIONS

This work examines the combustion behavior of single pulverized biomass particles from their ignition to their early stages of char oxidation. The biomass residues investigated were pine wood, wheat straw, rice husk and grape pomace. The biomass particles, in the size range 224-250

μm, were injected upward into a confined region with hot combustion products with a mean temperature of 1610 K and a mean O_2 concentration of 6.5 vol.%. Temporally and spectrally resolved images of the single burning particles were recorded with an ICCD camera equipped with different band-pass spectral filters. Data are reported for CH*, C_2*, Na* and K* chemiluminescence, and thermal radiation from soot and char burning particles.

The data on CH* and C_2* chemiluminescence and soot thermal radiation permits to identify important differences between the ignition delay time, volatiles combustion time and soot formation propensity of the four biomass residues, which are mainly affected by their volatile matter contents.

The Na* and K* emission signals follow the same trends of the CH* and C_2* emission signals from the ignition until the end of the volatiles combustion stage, beyond which the former persist owing to their release from the char burning particles, and the latter disappear owing to the end of the volatiles combustion stage. Furthermore, during the volatiles combustion stage, the Na*/CH* and K*/CH* ratios present constant values for each biomass residue.

Both the CH* and thermal radiation emission signals suggest that all biomass char particles experienced heterogeneous oxidation at or immediately after the extinction of the homogeneous volatiles combustion. In the case of the rice husk particles, the onset of the char oxidation stage occurs at the end of the volatiles combustion stage, while in the cases of the wheat straw and grape pomace particles, a slight overlap between the two stages is observed.

ACKNOWLEDGEMENTS

This work was financed by the Swedish Energy Agency through CECOST, the Knut and Alice Wallenberg foundation through grant KAW 2015.0294 and the European Research Council through Advanced Grant TUCLA, and by the Fundação para a Ciência e a Tecnologia (FCT) through IDMEC, under LAETA, project UID/EMS/50022/2013 and project PTDC/EMS-ENE/5710/2014. M. Costa also acknowledges FCT for the sabbatical leave grant SFRH/BSAB/128236/2016.

References

[1] W. Weng, M. Costa, Z. Li, M. Aldeń, Temporally and spectrally resolved images of single burning pulverized wheat straw particles, Fuel 224 (2018) 434-441.

[2] A. Molina, C.R. Shaddix, Proc. Combust. Inst. 31 (2007) 1905-1912.

[3] C.R. Shaddix, A. Molina, Proc. Combust. Inst. 32 (2009) 2091-2098.

[4] R. Khatami, C. Stivers, Y.A. Levendis, Combust. Flame 159 (2012) 3554-3568.

[5] J. Riaza, R. Khatami, Y.A. Levendis, L. Álvarez, M.V. Gil, C. Pevida, F. Rubiera, J.J. Pis, Combust. Flame 161 (2014) 1096-1108.

[6] R. Khatami, Y.A. Levendis, M.A. Delichatsios, Combust. Flame 162 (2015) 2508-2517.

[7] R. Khatami, Y.A. Levendis, Combust. Flame 164 (2016) 22-34.

[8] J. Köser, J.G. Becker, A.K. Goßmann, B. Böhm, A. Dreizler, Proc. Combust. Inst. 36 (2017) 2103-2111.

[9] J. Riaza, R. Khatami, Y.A. Levendis, L. Álvarez, M.V. Gil, C. Pevida, F. Rubiera, J.J. Pis, Biomass Bioenergy 64 (2014) 162-174.

[10] C. Mock, H. Lee, S. Choi, V. Manovic, Energy Fuels 30 (2016) 10809-10822.

[11] C. Mock, H. Lee, S. Choi, V. Manovic, Fuel 200 (2017) 467-480.

[12] G. Simões, D. Magalhães, M. Rabaçal, M. Costa, Proc. Combust. Inst. 36 (2017) 2235-2242.

[13] A. Carvalho, M. Rabaçal, M. Costa, M.U. Alzueta, M. Abian, Fuel 209 (2017) 787-794.

[14] M.J. Wornat, R.H. Hurt, N.Y.C. Yang, T.J. Headley, Combust. Flame 100 (1995) 131-143.

[15] M.J. Wornat, R.H. Hurt, K.A. Davis, N.Y.C. Yang, Proc. Combust. Inst. 26 (1996) 3075-3083.

Figure Captions

Figure 1. Schematic views of the (a) experimental setup; and (b) optical diagnostics for the capture of images of single burning particles.

Figure 2. Sequences of instantaneous images (left) and respective instantaneous emission signal areas (right) of the four burning pulverized biomass particles obtained with the ICCD camera equipped with the 430 nm band-pass filter as a function of the particle residence time in the hot combustion products region. (a) Pine wood (PW); (b) wheat straw (WS); (c) rice husk (RH); (d) grape pomace (GP). In the emission signal area curves, the location of the peak value and 15% of the peak value are indicated.

Figure 3. Particle velocity of the four burning pulverized biomass particles as a function of the residence time.

Figure 4. Average emission signal area (left) and emission signal value (right) of the four burning pulverized biomass particles obtained with the ICCD camera equipped with different pairs of filters as a function of the particle residence time in the hot combustion products region. (a) Emission signal area with 430 nm (CH*); (b) emission signal area with 515 nm (C_2*); (c) emission signal area with 652 nm (soot); (d) emission signal value with 430 nm (CH*); (e) emission signal value with 515 nm (C_2*); (f) emission signal value with 652 nm (soot).

Figure 5. Average emission signal area (left) and emission signal area ratio (right) of the four burning pulverized biomass particles obtained with the ICCD camera equipped with the pair of filters 589 nm/430 nm and 766 nm/430 nm as a function of the particle residence time in the hot combustion products region. (a) Emission signal area with 589 nm (Na*); (b) emission signal area with 766 nm (K*); (c) emission signal area ratio 589 nm/430 nm (Na*/CH*); (d) emission signal area ratio 766 nm/430 nm (K*/CH*).

Figure 6. Typical sequences of instantaneous images (left) and respective normalized instantaneous emission signal value (right) of three burning pulverized biomass particles obtained with the ICCD camera equipped with the pair of filters RG 1000/430 nm as a

function of the particle residence time in the hot combustion products region. (a) Wheat straw (WS); (b) rice husk (RH); (c) grape pomace (GP).